ACS Biomaterials SCIENCE & ENGINEERING

Article

pubs.acs.org/journal/abseba

Lyophilized Silk Sponges: A Versatile Biomaterial Platform for Soft Tissue Engineering

Jelena Rnjak-Kovacina,*[,†,‡] Lindsay S. Wray,[†] Kelly A. Burke,[†,§] Tess Torregrosa,[†] Julianne M. Golinski,[†] Wenwen Huang,[†] and David L. Kaplan[†]

[†]Department of Biomedical Engineering, Tufts University, 4 Colby Street, Medford, Massachusetts 02155, United States

[‡]Graduate School of Biomedical Engineering, UNSW Australia, Sydney, NSW 2052, Australia

[§]Chemical & Biomolecular Engineering Department, University of Connecticut, 191 Auditorium Road, Storrs, Connecticut 06269-3222, United States

Supporting Information

ABSTRACT: We present a silk biomaterial platform with highly tunable mechanical and degradation properties for engineering and regeneration of soft tissues such as, skin, adipose, and neural tissue, with elasticity properties in the kilopascal range. Lyophilized silk sponges were prepared under different process conditions and the effect of silk molecular weight, concentration and crystallinity on 3D scaffold formation, structural integrity, morphology, mechanical and degradation properties, and cell interactions in vitro and in vivo were studied. Tuning the molecular weight distribution (via degumming time) of silk allowed the formation of stable, highly porous, 3D scaffolds that held form with silk concentrations as low as 0.5% wt/v. Mechanical properties were a function of silk concentration and scaffold degradation was driven by beta-sheet content. Lyophilized silk sponges supported the adhesion of mesenchymal stem cells throughout 3D scaffolds, cell proliferation in vitro, and cell infiltration and scaffold remodeling when implanted subcutaneously in vivo.

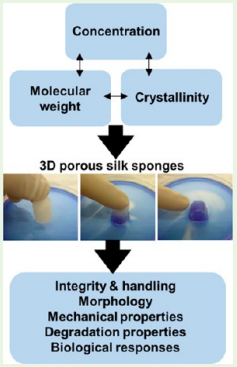

KEYWORDS: *silk, scaffold, soft tissue engineering, lyophilized sponge, biomaterial*

1. INTRODUCTION

Biomaterials play a central role in regenerative medicine and tissue engineering strategies. They serve as tunable biophysical and biochemical environments that direct cellular behavior and function and can thus be used to replace and regenerate missing or injured tissue, deliver cells, drugs, and biological molecules to the site of injury and study biological processes in vitro.[1]

Soft tissue loss and damage associated with trauma and disease, such as tumor resection and large traumatic injuries, present a significant healthcare burden worldwide. These are often complex wounds with damage to a number of tissue types, including muscle, skin, adipose, and neural tissues, and require biomaterial platforms with highly tunable physical features to accommodate the complex tissue defect. Soft tissue biomaterials need to be pliable to match the contours of the tissue defect, while offering adequate mechanical support to prevent the collapse of the defect. These systems also requires interconnected pores of 100−300 μm to allow exchange of gases and nutrients and infiltration of cells, as well as degradation rates that match the kinetics of de novo tissue formation.[1,2] Despite their drawbacks, most clinically used materials for soft tissue repair are based on synthetic polymers such as polypropylene and silicones or collagens from allogeneic and xenogeneic sources. Examples include bulking agents and meshes used to treat urinary incontinence, pelvic organ prolapse, and hernias, breast reconstruction implants, skin substitutes, and wound dressings for burn injuries and diabetic foot ulcers and injectable extracellular matrix preparations for muscle repair following sports or other traumatic injuries. These materials often result in inflammation, pain, and infection, as they were typically selected on the basis of previous regulatory approval, rather than optimal properties for the specific injury.[3]

Biomaterials also play an essential role in developing 3D, physiologically relevant in vitro models of soft tissues and complex soft tissue systems that are currently not well represented by 2D cell cultures on tissue culture plastic or glass substrates. In light of extensive evidence on the role of mechanotransduction on cell fate and tissue formation,[4,5] it is essential to develop biomaterials with physical properties better suited for soft tissue engineering.

In this study, we developed silk scaffolds with tunable mechanical and degradation properties for soft tissue engineering. Silk protein has emerged as a promising and versatile natural polymer for the development of biomaterial systems.[6−8] Regenerated silk is a cell compatible, biodegradable protein that can be engineered into a range of material formats, including porous scaffolds and sponges, hydrogels, films, fibers and microspheres.[8] Three-dimensional, porous silk scaffolds have been engineered using a range of methods including salt

Received: December 4, 2014
Accepted: February 25, 2015
Published: February 25, 2015

DOI: 10.1021/ab500149p
ACS Biomater. Sci. Eng. 2015, 1, 260−270

leaching, gas foaming and lyophilization.[9] Of these, salt leached scaffolds have gained significant attention because of their potential for bone tissue engineering and regeneration.[10−13] However, although many avenues have been explored for engineering stiffer and stronger salt-leached silk scaffolds, this method has limited parameters for developing scaffolds with appropriate mechanical and degradation properties for engineering soft tissues such as muscle, adipose or neural tissues.

Lyophilized silk sponges are prepared by freezing and lyophilizing an aqueous silk solution to generate soft, porous sponges. Ice crystals formed during the freezing process sublime, leaving pores where crystals were previously present.[14] All material processing steps in this method are performed under aqueous conditions in the absence of harmful solvents and the use of water, rather than sodium chloride as a porogen, allows for control over scaffold crystallinity and thus degradation properties.[15]

In this study, we investigated the properties of lyophilized silk sponges prepared under different process conditions, with the aim of developing a versatile biomaterial platform with tunable mechanical and degradation properties for use in soft tissue engineering and regenerative medicine. In particular, we studied the effect of silk molecular weight (degumming time), concentration, and crystallinity (beta-sheet content) on scaffold formation, structural integrity, morphology, mechanical and degradation properties, and cell interactions in vitro and in vivo.

2. MATERIALS AND METHODS

2.1. Silk Solution Preparation. Silk fibroin solution was prepared as reported previously.[8] Briefly, pure silk fibroin was extracted from *Bombyx mori* cocoons by degumming the fibers in a sodium carbonate solution (0.02 M) (Sigma-Aldrich, St. Louis, MO) for 5, 10, 30, or 60 min to remove sericin. Adequate level of sericin removal via short degumming time (5 min) has previously been demonstrated.[16] The pure silk fibroin was solubilized in aqueous lithium bromide (9.3 M) (Sigma-Aldrich, St. Louis, MO) for 4 h at 60 °C. Five and ten minute degummed silk fibers were dissolved in lithium bromide solution at 20% wt/v, whereas 30 and 60 min degummed fibers were dissolved at 25% wt/v. The solution was dialyzed using D-Tube Dialyzers (3500 MWCO, EMD Millipore, Billerica, MA) against deionized water until the conductivity of the dialysis water was <10 μS cm^{-1} (indicative of complete lithium bromide removal). The concentration of the silk solution was determined by drying a known volume of the solution and massing the remaining solids. This protocol resulted in a 6−8% wt/v silk solution. Silk solutions were stored at 4 °C.

2.2. Analysis of Silk Molecular Weight. Differences in silk molecular weight (MW) resulting from different fiber degumming times were visualized with sodium dodecyl sulfate polyacrylamide gel electrophoresis (SDS-PAGE). For each sample, 50 μg of solubilized silk protein was loaded into a 3−8% Tris Acetate Novex gel (NuPAGE, Invitrogen, Carlsbad, CA) under reducing conditions. The gel was run at 200 V for 45 min with a high molecular weight ladder (HiMark Unstained, Invitrogen) and then stained with a Colloidal Blue staining kit (Invitrogen). Protein distribution was quantified by taking densitometric measurements along the length of the gel (ImageJ, NIH, Bethesda, MD) as previously described.[16]

2.3. Preparation of Lyophilized Silk Sponges. Aqueous silk solution (0.5−4% wt/v in deionized water) was dispensed into wells of standard 24-well cell culture plates (3 mL/well) for all studies, other than mechanical testing, where larger scaffolds were required and were thus cast in custom-made 20 mm × 20 mm × 20 mm Teflon molds (5 mL/mold). Silk was frozen overnight at −20 °C in a standard laboratory freezer and lyophilized at −80 °C for 48h. Dry scaffolds were removed from the molds and rendered insoluble in aqueous environments by either water annealing[15] at room temperature for 30 min, 2h, 6h or 24h or autoclaving at 121 °C for 20 min at 15 psi to induced β-sheet formation. Scaffolds were rehydrated in deionized water or phosphate buffered saline (PBS) prior to further analyses. A dense, nonporous "skin" was formed at the top surface of each scaffold and was removed prior to further analyses (by peeling the skin away immediately postlyophilization using forceps or by cutting the skin away using a razor blade).

2.4. Characterization of Scaffold Crystallinity (Beta-Sheet Content). Fourier transform infrared spectroscopy (FTIR) analysis was performed to quantify the beta-sheet content of scaffold prepared under different conditions. Analyses were performed using an FT/IR-6200 Spectrometer (Jasco, Easton, MD), equipped with a triglycine sulfate detector in attenuated total reflection (ATR) mode. For each measurement, 64 scans were coadded with resolution 4 cm^{-1}, and the wave numbers ranged from 600 to 4000 cm^{-1}. The background spectra were collected under the same conditions and subtracted from the scan for each sample. Fourier Self-Deconvolution (FSD) of the infrared spectra covering the Amide I region (1595−1705 cm^{-1}) was performed with Opus 5.0 software (Bruker Optics Corp., Billerica, MA), as described previously.[17] The deconvoluted Amide I spectra were area-normalized, and the relative areas of the single bands were used to determine the fraction of the secondary structural elements in scaffolds.[18]

2.5. Characterization of Scaffold Stability and Integrity. The effect of different beta-sheet induction methods (water annealing for 30 min, 2 h, 6 h, or 24 h, or autoclaving for 20 min) on silk scaffold stability, volume and density was assessed.[15] Scaffold dimensions (height, diameter) and mass were recorded following lyophilization, beta-sheet induction and rehydration and scaffold volume (cm^3) and density (g/cm^3) were calculated. Scaffold integrity under different molecular weight (5−60 min degumming time) and beta-sheet induction (2h water annealing vs autoclaving) conditions was assessed independently by two researchers to score structural integrity and ease of handling, as well as the extent to which scaffolds retained their size and shape following hydration.

2.6. Characterization of Scaffold Morphology. Scaffold morphology was visualized by scanning electron microscopy (SEM). To maintain sample structure in the dry state, we froze the rehydrated scaffolds at −80 °C and lyophilized them for 12 h prior to imaging. Dried samples were sputter-coated with platinum/palladium (40 mA, 60 s) and imaged with a field-emission SEM and 5 kV electron beam (Supra55VP, Zeiss, Oberkochen, Germany).

2.7. Characterization of Scaffold Mechanical Properties. The mechanical properties of silk sponges were characterized using a TA Instruments RSA III dynamic mechanical analyzer. Scaffolds were cut to 20 mm × 2 mm × 3 mm (height x width x thickness), loaded into tension clamps such that the sample's initial gauge length was 10 mm, and submerged in a bath of PBS at room temperature. Samples were elongated at a rate of 0.1 mm/s (strain rate 1%/s) until failure, and data was collected using TA Orchestrator Software version 7.2.0.2 from TA Instruments (New Castle, DE). Young's modulus was calculated on scaffolds that failed in the middle of the sample at 5−10% strain. At least n = 4 samples were used to calculate average modulus with standard deviation.

2.8. Characterization of Scaffold Degradation in Vitro. In vitro degradation of silk scaffolds was analyzed as previously described.[17] Briefly, silk scaffolds (12 mm diameter, 2 mm height) were placed in preweighted 1.5 mL Eppendorf tubes and dried at 60 °C. The mass of dry scaffolds was recorded and 1 mL of 1 U/mL Protease XIV solution (in PBS, Sigma-Aldrich, St. Louis, MO) was added to each tube and incubated at 37 °C. Every 2 days, Protease XIV was removed, samples were washed twice with deionized water and dried at 60 °C, and dry mass was recorded prior to addition of fresh Protease XIV solution. Scaffold degradation was calculated as % remaining mass compared to original scaffold mass. Control samples were incubated in PBS to baseline silk sponge degradation in the absence of Protease XIV.

2.9. Cell Interactions with Lyophilized Silk Sponges. Human mesenchymal stem cells (hMSCs) were isolated from fresh bone marrow aspirate (Lonza, Basel, Switzerland) as previously described.[19]

DOI: 10.1021/ab500149p
ACS Biomater. Sci. Eng. 2015, 1, 260−270

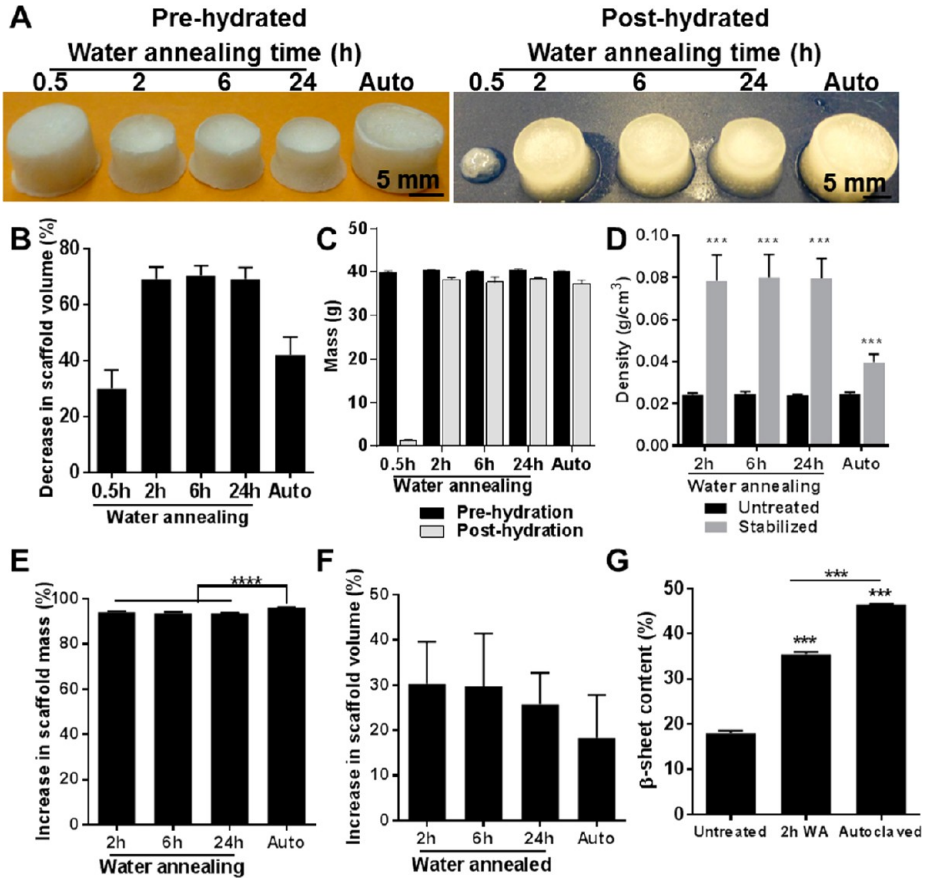

Figure 1. Silk sponge stabilization in the absence of cross-linking agents. (A) Lyophilized silk sponges pre- and posthydration (in water) following stabilization via water annealing for 0.5−24 h at room temperature or autoclaving for 20 min at 121 °C. (B) Percent decrease in silk sponge volume following water annealing or autoclaving stabilization treatments compared to as lyophilized scaffolds. (C) Lyophilized silk sponge mass pre- and posthydration following water annealing or autoclaving stabilization treatments. (D) Lyophilized silk sponge density (prehydration) pre- and post-water annealing or autoclaving stabilization treatments. (E) Lyophilized silk sponge hydration in water following water annealing or autoclaving stabilization treatments (percent increase in scaffold mass compared to scaffolds prior to hydration). (F) Lyophilized silk sponge hydration in water following water annealing or autoclaving stabilization treatments (percent increase in scaffold volume compared to scaffolds prior to hydration). (G) Lyophilized silk sponge crystallinity (beta-sheet content) pre- and post-water annealing or autoclaving stabilization treatments. Data are expressed as mean ± SD, $n = 6$ (except F, where $n = 3$), *** $p < 0.001$, **** $p < 0.0001$.

hMSCs (P3) were seeded on silk scaffolds (12 mm diameter, 2 mm height) at a cell density of 1.5×10^5 cells/scaffold in a total volume of 100 μL. Samples were incubated at 37 °C in 5% CO_2 for 2 h before media was added. The relative number of metabolically active cells within each scaffold was determined by the AlamarBlue (Life Technologies, Grand Island, NY) assay according to the manufacturer's instructions. Scaffolds were washed with PBS and incubated in medium with 10% AlamarBlue reagent for 2h at 37 °C with 5% CO_2. Following incubation, aliquots (100 μL) were transferred to black 96-well plates and quantified for fluorescence intensity with a fluorescence plate reader (SpectraMax M2, Molecular Devices, Sunnyvale, CA) using an excitation wavelength of 550 nm and an emission wavelength of 590 nm. Acellular scaffolds and tissue culture wells were also maintained in culture medium as above and were analyzed similarly as blank controls to adjust for background fluorescence.

At the end of the 15 day incubation period, scaffolds were stained with calcein AM (2 μM, Life Technologies, Grand Island, NY) for 45 min at 37 °C to stain live cells and imaged with a Leica DMIRE2 confocal laser scanning microscope (CLSM) with excitation at 488 nm and emission at 500−520 nm (Wetzlar, Germany).

For the cell infiltration study, cells were seeded at at $5-6 \times 10^3$ cells/mm^3 in a volume of fibrin that filled the entire void space of the scaffold (12 mm diameter, 10 mm height). Fibrin was prepared by mixing human fibrinogen (10 mg mL^{-1}) (EMD Millipore Chemicals, Billerica, MA) with human thrombin (5 U/mL) (Sigma-Aldrich, St. Louis, MO) in a 4:1 volume ratio. Scaffolds were cut along the scaffold length, stained with calcein AM, and imaged as described above.

2.10. In Vivo Implantation and Analyses of Lyophilized Silk Sponges. All procedures were conducted under animal care protocols approved by Tufts Institutional Animal Care and Use Committee. All animals used in this study were 6-week old BALB/c female mice (Charles River Laboratories, Wilmington, MA). Silk scaffolds (8 mm diameter, 2 mm height) were implanted in subcutaneous pockets of each mouse under general anesthesia of oxygen and isoflurane. At week 2, 6, or 12 postsurgery, animals were euthanized and the samples along with the overlaying tissue were collected for histological examination. Samples were fixed with 10% neutral buffered formalin (NBF) and embedded in paraffin following a series of xylene and graded ethanol incubations. Samples were sectioned to 6 μm thickness and deparaffinized. Sections were stained with hematoxylin and eosin (H&E, Sigma-Aldrich, St. Louis, MO).

2.11. Statistical Analyses. Data are expressed as mean ± standard deviation (SD). Statistically significant differences were determined by one- or two-way analysis of variance (ANOVA) and the Tukey post-test. Statistical significance was accepted at $p < 0.05$ and indicated in the figures as *$p < 0.05$, **$p < 0.01$, ***$p < 0.001$, and ****$p < 0.0001$.

DOI: 10.1021/ab500149p
ACS Biomater. Sci. Eng. 2015, 1, 260−270

3. RESULTS

3.1. Silk Sponge Stabilization in the Absence of Cross-Linking Agents. Lyophilized silk sponges were generated by freezing a 4% wt/v silk solution at −20 °C and lyophilizing at −80 °C (Figure 1A). Lyophilized sponges were not stable in aqueous condition without further treatment and dissolved completely upon contact with water or PBS (data not shown). To stabilize silk sponges in aqueous environments, sponges were water annealed (exposed to water vapor under vacuum) for 0.5, 2, 6, or 24 h or autoclaved for 20 min at 120 °C under a steam cycle. The volume of all samples decreased following water annealing (Figure 1A). Water annealing for 0.5, 2, 6, and 24 h reduced the scaffold volume by 29.98 ± 6.64%, 69.21 ± 4.26%, 70.43 ± 3.62%, and 69.31 ± 4.05%, respectively. Autoclaving reduced scaffold volume by 42.11 ± 6.36% (Figure 1B). All treatment conditions resulted in stable silk sponges, apart from 0.5h water annealing, which resulted in insufficient stabilization and partial scaffold dissolution when placed in water (Figure 1A). Following extended hydration in water, treated scaffold were dried and the remaining mass recorded (Figure 1C). All scaffolds displayed some level of mass loss, but the mass of 0.5 h water annealed sponges showed the greatest decrease of 96.95 ± 0.77%. The mass of 2, 6, and 24 h water annealed sponges decreased by 5.15 ± 0.55%, 6.03 ± 2.91%, and 4.62 ± 1.11%, respectively. The mass of autoclaved sponges decreased by 6.51 ± 1.74%.

Because of poor silk sponge stabilization following water annealing for 0.5 h, this condition was not considered further. Considering the small loss of silk following stabilization under all other conditions, the decrease in scaffold volume indicated that silk sponges underwent densification. The density of all sponges increased significantly ($p < 0.001$) following water annealing (Figure 1D). However, once exposed to water, all scaffolds hydrated easily, with sponges water annealed for 2 h, 6h and 24h increasing in mass by 94.23 ± 0.36%, 93.68 ± 0.57%, and 93.68 ± 0.28%, respectively (i.e., sponges took up 17.4 ± 1.1, 15.9 ± 1.4, and 15.9 ± 0.7 times their mass in water), while autoclaved scaffolds hydrated significantly better ($p < 0.001$), increasing in mass by 96.20 ± 0.26% (i.e., taking up 26.4 ± 1.8 times their weight in water) (Figure 1E). The volume of all silk sponges also increased posthydration in water, with 2, 6, and 24 h water annealed sponges increasing in volume by 30.25 ± 9.37%, 29.77 ± 11.67% ,and 25.80 ± 6.89%, respectively, and autoclaved scaffold volume increasing by 18.33 ± 9.51% (Figure 1F).

No differences in scaffold integrity, handling, and hydration were observed between water annealing treatments, and so 2 h was selected for all other studies and compared to autoclaving. Both treatments resulted in a significant increase in crystallinity compared to untreated lyophilized sponges, with beta-sheet content increasing from 18.0 ± 0.5% in the untreated samples to 35.5 ± 0.5% ($p < 0.001$) in 2h water annealed and 46.5 ± 0.1% ($p < 0.001$) in autoclaved samples (Figure 1G). The beta-sheet content of autoclaved samples was significantly higher than that of 2 h water annealed samples ($p < 0.001$).

3.2. Porosity and Pore Morphology of Lyophilized Silk Sponges. SEM analysis of lyophilized silk sponges revealed a network of thin, sheet-like lamellae with interconnected porosity. Water annealed and autoclaved scaffolds displayed similar morphology (Figure 2A). As the pores of lyophilized sponges appeared highly interconnected without defined pore boundaries, pore size was not quantified,

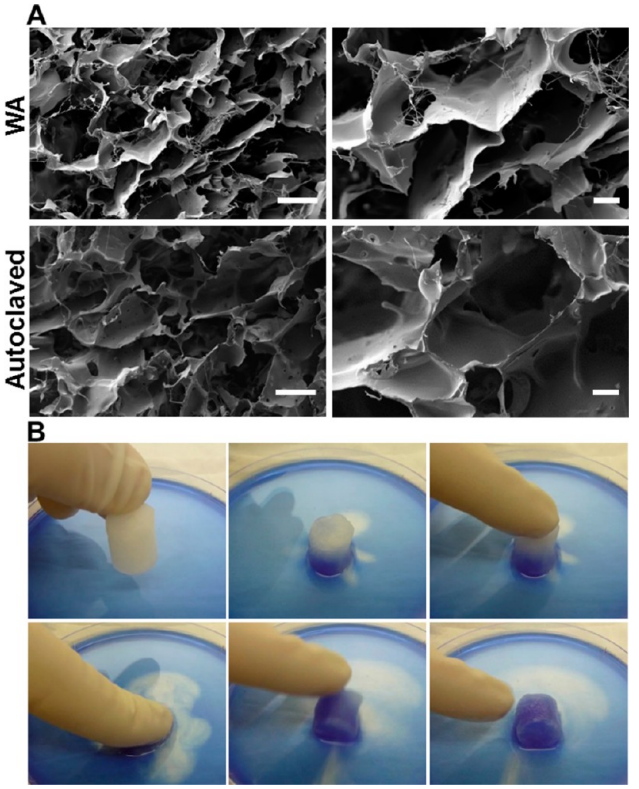

Figure 2. Porosity and pore morphology of lyophilized silk sponges. (A) SEM micrographs of lyophilized silk sponges following water annealing (2h) or autoclaving stabilization treatments and showing a network of thin, sheetlike lamellae with interconnected porosity. Scale bars are 200 μm in images on the left and 50 μm in images on the right. (B) Lyophilized silk sponge stabilized by autoclaving and hydrated in PBS was placed in a dish containing blue dye to demonstrate the soft, compliant nature of the biomaterial and dye movement through the pores and thus pore interconnectivity.

but the distance between adjacent lamellae appeared to be ∼100−400 μm in SEM images (Figure 2A). To demonstrate pore interconnectivity, we rehydrated an autoclaved lyophilized sponge in PBS and placed it in a dish containing Alamar blue dye. Immediately upon contact with the dye, the bottom half of the sponge appeared blue, despite already being hydrated in PBS. When the sponge was squeezed with a finger and released, the PBS in the sponge was replaced with the blue dye, coloring the entire sponge blue and indicating that the dye moved from the bottom of the sponge throughout the entire construct, as well as the soft, compliant nature of the lyophilized silk sponges (Figure 2B). Pore interconnectivity was further demonstrated by pipetting blue dye on the top surface of the sponge and observing dye movement throughout the sponge (Figure S1 in the Supporting Information) and homogeneous cell distribution when cells were seeded in lyophilized silk sponges (see Section 3.6).

3.3. Screening the Physical Properties of Lyophilized Silk Sponges. To develop a comprehensive biomaterial platform with physical properties that can be tuned for different soft tissue engineering and regenerative medicine applications, we studied the effect of silk concentration and molecular weight on the final scaffold properties.

Lyophilized silk sponges were cast from 4, 2, 1, and 0.5% wt/v silk solution (Figure 3A). All silk concentrations resulted in freestanding, soft sponges that retained the shape of the casting

DOI: 10.1021/ab500149p
ACS Biomater. Sci. Eng. 2015, 1, 260−270

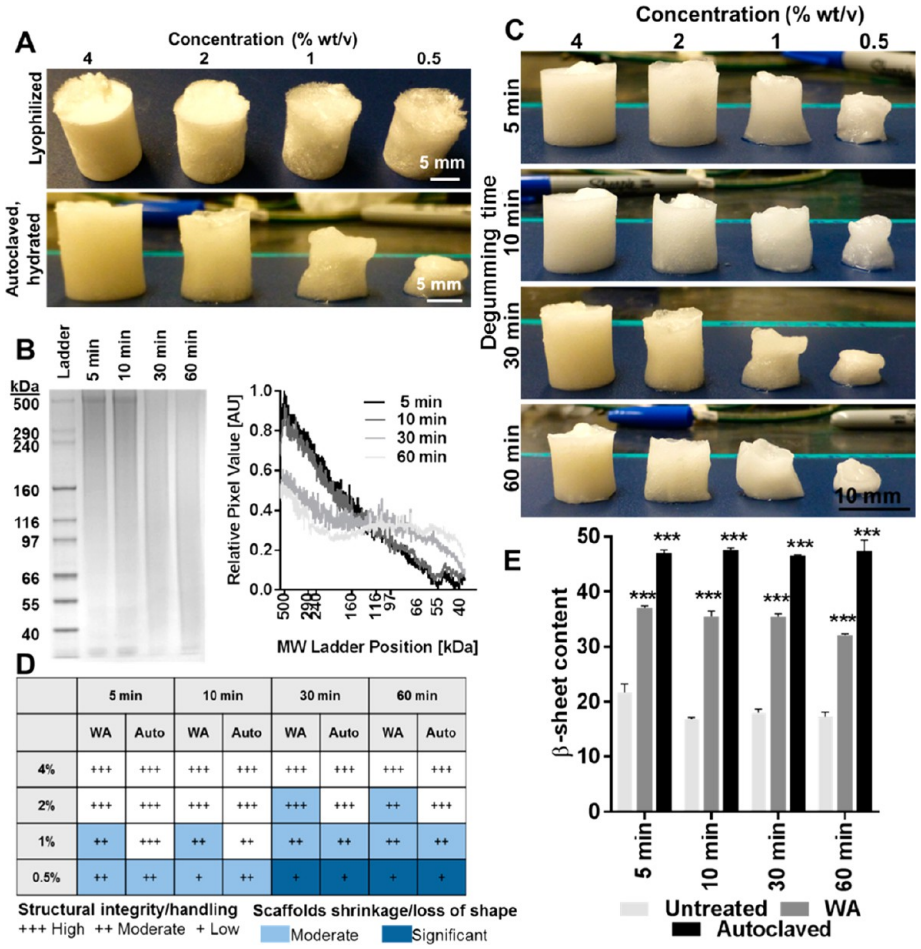

Figure 3. Effect of silk concentration and molecular weight distribution on the physical properties of lyophilized silk sponges. (A) Lyophilized silk sponges cast from 30 min degummed silk at 4, 2, 1, and 0.5% wt/v pre- and posthydration (in water) following stabilization via autoclaving. (B) SDS-PAGE analysis of silk molecular weight following different degumming times (5−60 min). (C) Lyophilized silk sponges cast from silk degummed for 5−60 min at 0.5−4% wt/v following hydration in PBS. (D) Comprehensive study showing "structural integrity/handling" and "scaffold shrinkage and loss of shape" scores of lyophilized silk sponges cast from silk degummed for 5−60 min at 0.5−4% wt/v and stabilized by 2 h water annealing or autoclaving (hydrated in PBS). (E) Lyophilized silk sponge crystallinity (beta-sheet content) cast from 5 to 60 min degummed silk and post-water annealing or autoclaving stabilization treatments. Data are expressed as mean ± SD, $n = 3$, *** $p < 0.001$.

mold. Sponges with low silk concentration (0.5 and 1% wt/v) were more fragile and difficult to handle, as they deformed under small loads more easily compared to higher concentration scaffolds (2 and 4% wt/v). In the dry state, low concentration silk sponges were not brittle. Upon hydration, however, low concentration silk sponges did not retain their shape as well as high concentration scaffolds and 0.5% wt/v scaffolds collapsed under their own weight and it was difficult to pick up and handle the samples (Figure 3A).

We hypothesized that scaffolds of higher molecular weight would maintain their shape and ease of handling at lower silk concentrations. To test this hypothesis, we performed a study to assess the effect of scaffold concentration and molecular weight on scaffold integrity, ease of handling, and maintenance of scaffold shape and size. Silk was degummed (boiled in sodium carbonate to remove sericin protein from the silk fiber) for 5, 10, 30, or 60 min to generate silk protein with different molecular weight distributions (Figure 3B). SDS-PAGE analysis of silk molecular weight distribution following different degumming times revealed that silk migrated as a polydisperse population with distinct bands observed only in 5 min and 10 in boiled silk at ∼500 kDa. SDS-PAGE analysis revealed two distinct silk populations based on molecular weight distribution (Figure 3B). Five min and 10 min boiled silk (high-molecular-weight silk, HMWS) had a size distribution predominantly above 160 kDa, while 30 and 60 min boiled silk (low molecular weight silk, LMWS) had a size distribution predominantly below 160 kDa.

Lyophilized sponges were cast from 5, 10, 30, and 60 min boiled silk at 4, 2, 1, and 0.5% wt/v concentrations. All conditions resulted in scaffolds that retained the shape of the mold except for the 60 min scaffolds at 0.5% and 1%, which formed scaffolds smaller than the original mold. A decrease in molecular weight (i.e., longer degumming time) and a decrease in scaffold concentration resulted in scaffolds that were more difficult to handle and did not retain their shape and size following hydration. All scaffolds, regardless of molecular weight, reduced in size following hydration at concentrations lower than 2% wt/v. However, scaffolds cast from HMWS retained their shape and ease of handling much better at low concentrations compared to LMWS (Figure 3C, D). The 0.5% and 1% wt/v scaffolds cast from HMWS retained their shape and could be picked up with forceps without collapsing even when hydrated. In addition to molecular weight distribution,

DOI: 10.1021/ab500149p
ACS Biomater. Sci. Eng. 2015, 1, 260−270

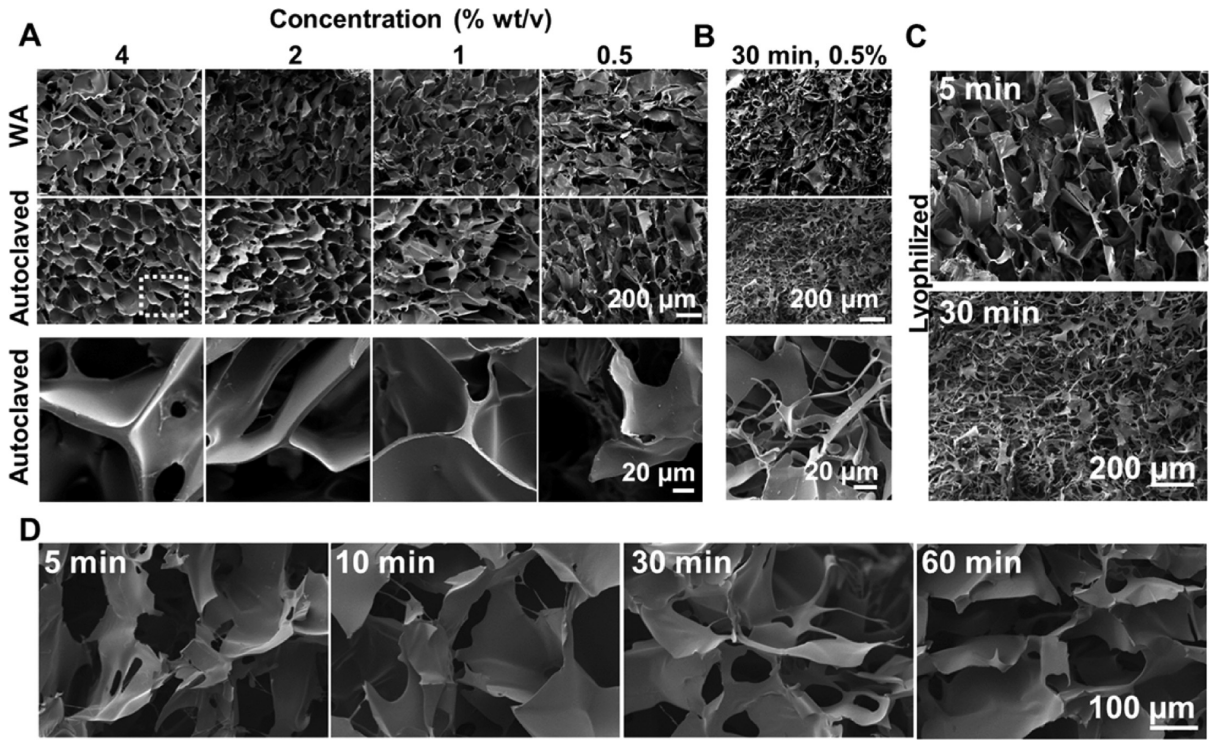

Figure 4. Effect of silk concentration and molecular weight on scaffold lamellae and pore morphology. (A) SEM micrographs of lyophilized silk sponges cast from 5 min degummed silk at 0.5−4% wt/v stabilized by 2 h water annealing or autoclaving, showing intact lamellae and interconnected pores. The bottom row shows decreased lamellae thickness with decreasing silk volume. (B) SEM micrographs of lyophilized silk sponges cast from 30 min degummed silk at 0.5% wt/v stabilized by 2 h water annealing or autoclaving showing collapsed pores and noncontinuous lamellae. (C) SEM micrographs of lyophilized silk sponges cast from 5 or 30 min degummed silk at 0.5% wt/v prior to stabilization showing that 5 min degummed silk resulted in formation of continuous, distinct lamellae, whereas the lamellae and pores of 30 min degummed scaffolds collapsed during lyophilization. (D) SEM micrographs of lyophilized silk sponges cast from 5 to 60 min degummed silk at 2% wt/v, showing that a higher concentrations (>1% wt/v), molecular weight does not affect pore and lamellae morphology.

beta-sheet content contributed to scaffold integrity, as autoclaved scaffolds were easier to handle and maintained better scaffold integrity compared to 2 h water annealed scaffolds at all concentrations. Stabilization treatment (water annealing vs autoclaving) was the main factor for crystallinity, as there was no difference in beta-sheet content across the different molecular weights (Figure 3F).

SEM analysis of silk sponges formed from HMWS revealed highly porous scaffolds with interconnected pores and a trend toward thinner lamellae with decreasing silk concentration (Figure 4A). All sponges cast from HMWS formed porous networks, whereas sponges formed from LMWS displayed collapsed lamellae (thin, fibrous strands of protein, rather than sheet-like lamellae) and a heterogeneous pore network at 0.5% wt/v (Figure 4B). These lamellae and the pore network collapsed during lyophilization, as demonstrated by the LMWS sponge morphology prior to hydration (Figure 4C). At concentrations where intact lamellae did form (e.g., 2% wt/v), SEM analysis revealed no morphological differences between silk sponges cast from 5, 10, 30, or 60 min degummed silk (Figure 4D).

3.4. Tuning the Mechanical Properties of Lyophilized Silk Sponges. To elucidate the effect of different silk properties (molecular weight distribution, beta-sheet, and concentration) on the mechanical properties of lyophilized scaffolds, Young's modulus, ultimate tensile strength (UTS), and strain at break of silk scaffolds under tension were studied.

The effect of molecular weight was studied in 2% wt/v autoclaved (high beta-sheet content) scaffolds and revealed a power relationship between degumming time and the Young's modulus and UTS (Figure 5A). As the degumming time increased (and thus molecular weight decreased), the Young's modulus and UTS of silk scaffolds decreased. Although the small number of points does not allow for a robust trend to be established, the power relationship indicated that changes in molecular weight had a greater effect on the mechanical properties of silk in the HMWS population, compared to the LMWS population. Indeed, deceasing degumming time from 10 to 5 min, resulted in a ∼1.7 fold change in Young's modulus, compared to ∼1.3 fold change when degumming time was decreased from 60 to 30 min. The Young's modulus of 2% wt/v scaffolds ranged from 37.25 ± 7.50 kPa (60 min) to 142.80 ± 51.72 kPa (5 min), whereas UTS ranged from 8.68 ± 1.31 kPa (60 min) to 57.67 ± 30.72 kPa (5 min) and strain at break ranged from 25.19 ± 1.74% (60 min) to 54.32 ± 15.01% (10 min) (Figure 5A).

The effect of silk concentration was studied using autoclaved sponges cast from HMWS (5 min degumming) and LMWS (30 min degumming). Silk sponges were cast at 4, 2, 1, and 0.5% wt/v, but LMWS cast at 1 and 0.5% wt/v did not generate scaffolds robust enough for mechanical studies. A linear relationship was observed between silk concentration and mechanical properties, with Young's modulus and UTS increasing linearly with silk concentration (Figure 5B). The Young's modulus ranged from 44.50 ± 18.08 (0.5% wt/v) to 321.33 ± 49.38 (4% wt/v), whereas UTS ranged from 28.2 ± 11.92 kPa (0.5% wt/v) to 102.73 ± 23.19 kPa (4% wt/v) and strain at break ranged from 44.25 ± 8.97% (4% wt/v) to 60.11

DOI: 10.1021/ab500149p
ACS Biomater. Sci. Eng. 2015, 1, 260−270

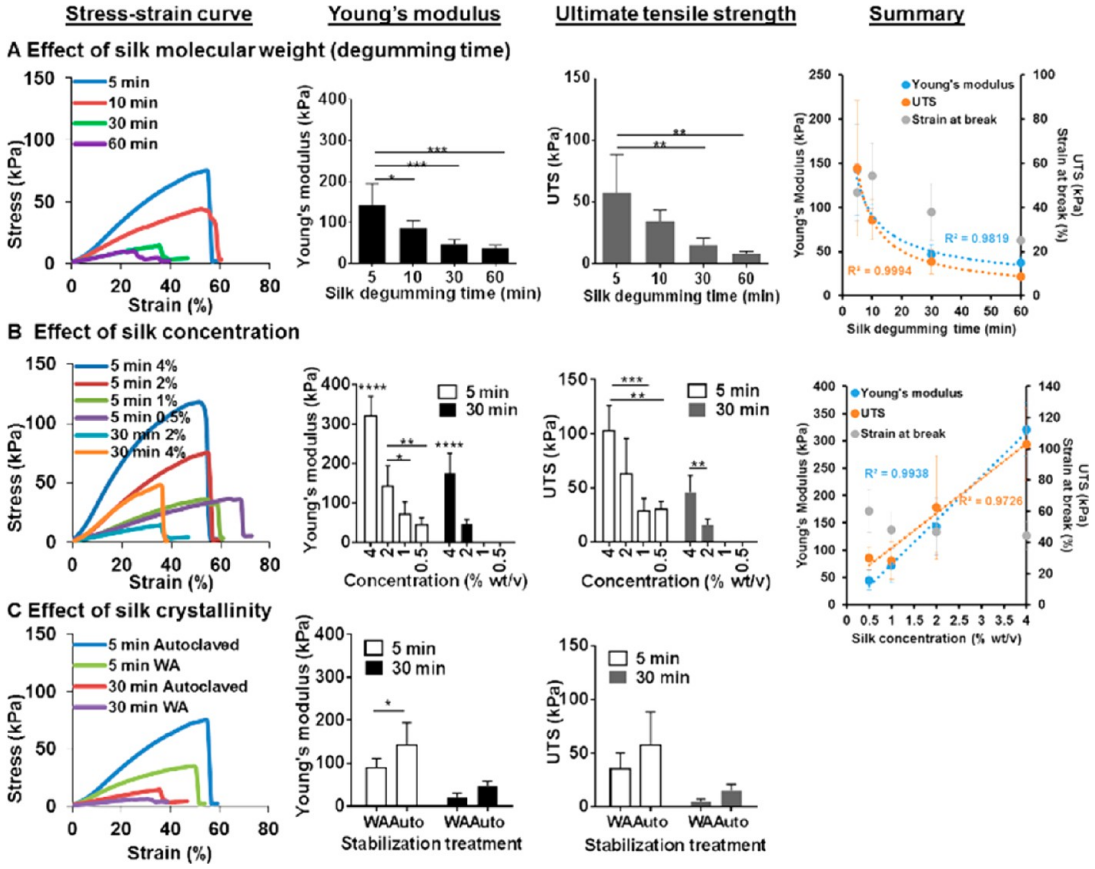

Figure 5. Mechanical properties of lyophilized silk sponges, showing stress−strain curves, Young's modulus, and ultimate tensile strength (UTS) generated from a tensile extension test. (A) Effect of silk molecular weight (degumming time) tested on 2% wt/v silk sponges cast from 5 to 60 min degummed silk and stabilized by autoclaving. (B) Effect of silk concentration tested on silk sponges cast from 5 min degummed silk (0.5−4% wt/v) and 30 min degummed silk (2−4% wt/v) stabilized by autoclaving. (C) Effect of silk crystallinity tested with 2% wt/v scaffolds cast from 5 or 30 min degummed silk and stabilized by 2 h water annealing (low beta-sheet content) or autoclaving (high beta-sheet content). Data are expressed as mean ± SD, n = 4−7, * $p < 0.05$, ** $p < 0.01$, *** $p < 0.001$.

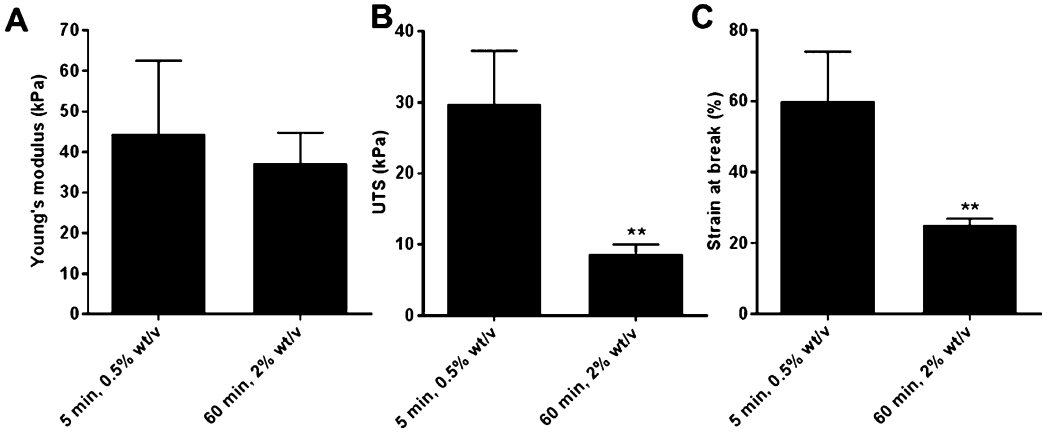

Figure 6. Effect of silk concentration and molecular weight on mechanical properties of lyophilized silk sponges. Comparison of mechanical properties of lyophilized silk sponges cast from high molecular weight (5 min degumming time) silk at low concentration (0.5% wt/v) with sponges cast from low molecular weight silk (60 min degumming time) at high concentration (2% wt/v). (A) Young's modulus, (B) ultimate tensile strength (UTS), and (C) strain at break generated from a tensile extension test. Data are expressed as mean ± SD, n = 4−7, ** $p < 0.01$.

± 13.90% (0.5% wt/v) for HMWS sponges. LMWS sponges displayed lower Young's modulus and UTS for corresponding concentration, but displayed a similar trend of decreased values with decreasing silk concentration. Interestingly, a change in silk concentration from 4% wt/v to 2% wt/v using HMWS had a smaller effect on mechanical properties (~1.82-fold decrease in Young's modulus and ~2.24-fold decrease in UTS) compared to the same concentration decrease using LMWS (~3.05-fold decrease in Young's modulus and ~4.06-fold decrease in UTS).

The effect of silk crystallinity (beta-sheet content) was investigated by comparing 2% wt/v autoclaved (high beta-

DOI: 10.1021/ab500149p
ACS Biomater. Sci. Eng. 2015, 1, 260−270

sheet) and water annealed (low beta-sheet) scaffolds cast from HMWS (5 min degumming) and LMWS (30 min degumming). Although a trend toward higher Young's modulus and UTS was observed in high crystallinity samples, a significant difference was only observed between the Young's moduli of autoclaved and water annealed sponges cast from HMWS (Figure 5C).

Finally, the mechanical properties of the "softest" scaffolds that showed mechanical robustness and ease of handling, namely sponges cast from 5 min degummed silk at 0.5% wt/v and 60 min degummed silk at 2% wt/v (both sets were autoclaved to induce beta-sheet formation) were compared. The scaffolds did not show a difference in Young's modulus ($p > 0.05$), but sponges cast from 5 min degummed silk showed significantly higher UTS ($p < 0.01$) and strain at break ($p < 0.01$) compared to sponges cast from 60 min degummed silk (Figure 6).

3.5. Tuning the Degradation Properties of Lyophilized Silk Sponges. To elucidate the effect of silk molecular weight, beta-sheet content, and concentration on the degradation properties of lyophilized scaffolds, we studied in vitro silk degradation in the presence of Protease XIV. Protease XIV is a cocktail of bacterial proteases that has been extensively used to study silk degradation[15,20,21] and can be useful to elucidate the relative effect of different silk properties on the degradation of silk sponges. Silk degradation was assessed as percent remaining mass after 2, 4, 6, or 8 days of exposure to Protease XIV. To study the effect of molecular weight on silk degradation, we cast silk sponges from 5, 10, 30, or 60 min degummed silk at 2% wt/v and stabilized by either water annealing (low beta-sheet content) or autoclaving (high beta-sheet content). At low beta-sheet content, accelerated silk degradation correlated with lower molecular weight, with 30 and 60 min scaffolds degrading completely by day 8, whereas 10 and 5 min scaffolds had 8.48 ± 8.94% and 26.56 ± 11.60% of original mass remaining. At high beta-sheet content, however, there was no correlation between silk molecular weight and degradation, but an overall decrease in the silk sponge degradation rate was observed, with ∼50% of original mass remaining in all scaffolds at day 8 (Figure 7A, B).

Similar trends were observed for silk concentration (scaffolds were cast from 5 min degummed silk), where accelerated silk degradation correlated with lower concentration at low beta-sheet, but to a much lesser extent at high beta-sheet content (Figure 7C, D).

3.6. Effect of Silk Properties on Cell Interactions. The effect of silk molecular weight and concentration on cell interactions with silk sponges was investigated using human bone marrow derived mesenchymal stem cells (hMSCs). hMSCs were seeded on 2% silk sponges cast from 5 or 30 min degummed silk or on scaffolds cast from 5 min degummed silk at different concentrations (4, 2, 1, and 0.5% wt/v) and cell metabolic activity was assessed at day 1, 5, 10, and 15 postseeding. Cells adhered and spread on all silk sponges and no significant difference in cell proliferation was observed on the different silk scaffolds (Figure 8). At day 15 postseeding, cells were stained with calcein AM and differences in cell morphology were observed with different silk concentrations. Cells on 4% wt/v silk scaffolds appeared larger and more spread compared to cells seeded on 0.5% wt/v scaffolds, and also followed the contours of the scaffold pores (Figure 8C). The interconnectivity of the scaffold pores was further confirmed by seeding cells on large (10 mm height) scaffolds (cells seeded from both sides) and visualizing cell infiltration 24 h postseeding using calcein AM staining. Homogenous cell distribution was observed throughout the scaffold (Figure 8D).

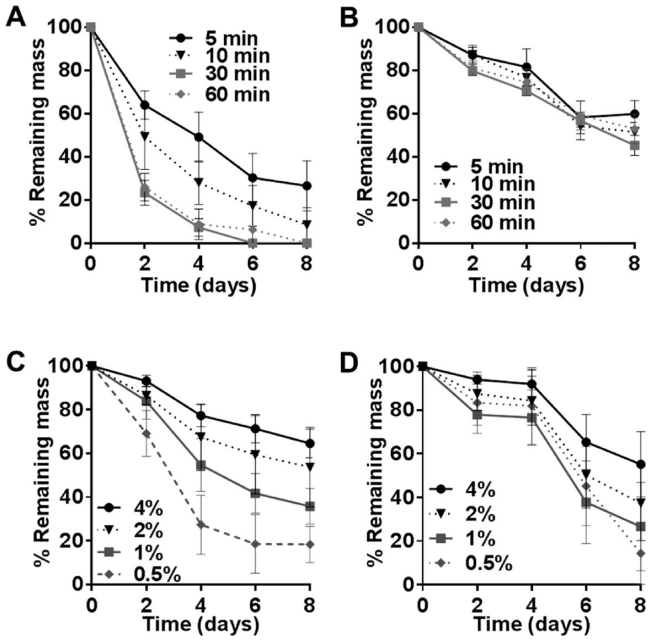

Figure 7. Effect of (A, B) molecular weight and (B, C) concentration on in vitro enzymatic degradation of lyophilized silk sponges. All curves show % remaining mass of scaffolds over an 8 day time period when incubated in Protease XIV at 37 °C. Protease XIV solution was changed every 2 days. (A, B) Degradation of 2% wt/v scaffolds cast from 5 to 60 min degummed silk stabilized by 2 h (A) water annealing or (B) autoclaving. (C, D) Degradation of silk sponges cast from 5 min degummed silk at 0.5−4% wt/v stabilized by 2 h (C) water annealing or (D) autoclaving. Data are expressed as mean ± SD, n = 5−7.

3.7. In Vivo Implantation of Lyophilized Silk Sponges. Silk sponges (8 mm diameter, 2 mm thickness) cast from 5 min or 30 degummed silk (2% wt/v, high beta-sheet content) were implanted subcutaneously in mice for 2, 6, or 12 weeks. Cells infiltrated into silk sponges from the scaffold periphery (∼500 μm thick cell layer on each side at week 2). By week 6 postimplantation, cells had infiltrated the scaffold, with areas of silk scaffold breakdown observed throughout. At week 12 postimplantation, silk scaffolds were degraded and cells were observed throughout most of the samples (Figure 9A). No obvious differences were observed in the morphology, cell infiltration or breakdown of the silk sponges cast from 5 or 30 min degummed silk. The thickness of the intact scaffold layer (as measured from H&E stained histological sections) was measured in each sample to assess silk degradation over time. Relative comparisons were only made between implanted samples, rather than compared to original scaffold thickness, as histological processing is known to cause sample shrinkage. A significant decrease in intact scaffold thickness was observed between weeks 2 and 6 ($p < 0.001$) and weeks 6 and 12 ($p < 0.01$ for 5 min degummed samples and $p < 0.001$ for 30 min degummed samples) (Figure 9B). However, no significant difference in scaffold thickness was observed between samples cast from 5 and 30 min degummed silk at different time points.

DOI: 10.1021/ab500149p
ACS Biomater. Sci. Eng. 2015, 1, 260−270

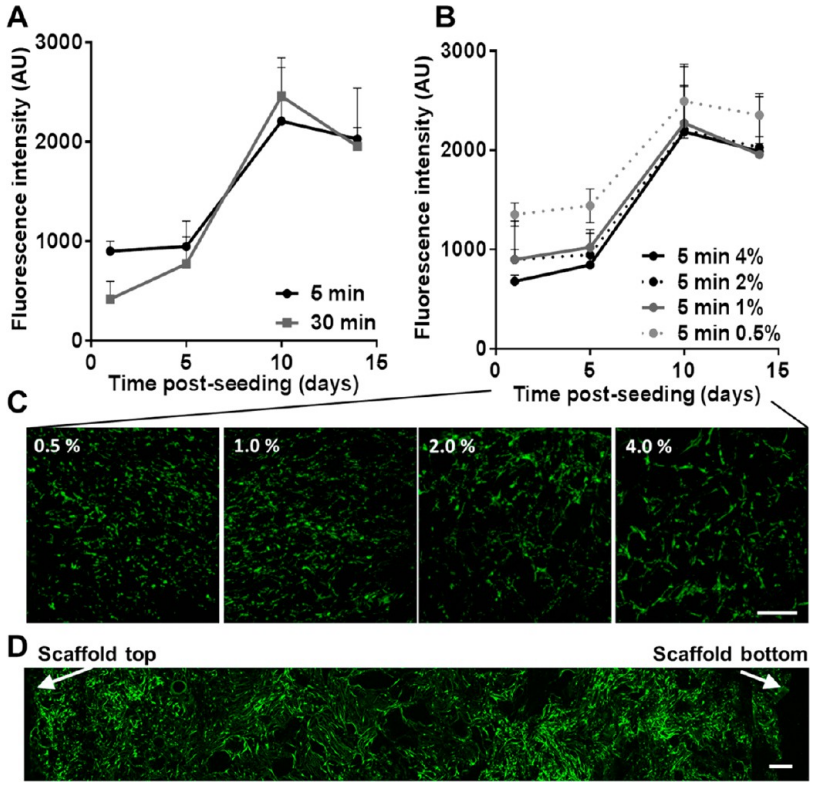

Figure 8. Cell interactions with lyophilized silk sponges in vitro. Alamar blue (metabolic activity) analysis of hMSC proliferation over a 15 day period on lyophilized silk sponges cast from (A) 5 or 30 min degummed silk at 2% wt/v stabilized by atutoclaving or (B) 5 min degummed silk at 0.5−4% wt/v stabilized by autoclaving. Data are expressed as mean ± SD, $n = 5$. (C) Confocal imaging of calcein AM (live cells, green) staining of hMSCs on lyophilized silk sponges cast from 5 min degummed silk at 0.5−4% wt/v (stabilized by autoclaving) at day 15 postseeding. (D) Cell infiltration in lyophilized silk sponges in vitro. Scaffolds (12 mm diameter, 10 mm height) were seeded with hMSCs and incubated for 24 h, sliced down the centerline along the long axis and stained with calcein AM. Representative fluorescent images along the middle of scaffold. Scale bars are 300 μm.

4. DISCUSSION

Silk materials have traditionally been engineered as strong, stiff, and mechanically robust constructs aimed at repairing, regenerating or studying hard tissues such as bone.[11,13,22] One of the most studied silk material formats are porous scaffolds prepared by leaching sodium chloride crystals of different sizes from the silk construct. However, although these materials are appropriate for engineering harder tissues, the high stiffness and slow degradation make them less suitable for some soft tissue engineering and regeneration needs. In this study, we utilized silk molecular weight (degumming time), concentration, and crystallinity parameters to develop a highly tunable biomaterial platform for soft tissue engineering. A strong interplay and codependence was found between processing parameters and the final scaffold properties, but general trends observed showed that the physical properties of lyophilized silk sponges can be tuned.

Lyophilized silk sponges formed as a network of thin, sheetlike lamellae with highly interconnected pores. This methodology allowed scaffold formation at much lower silk concentrations compared to salt leaching (0.5−4% wt/v lyophilized sponges compared to 4−17% wt/v salt-leached scaffolds).[9,23] Scaffold integrity and ease of handling decreased with decreasing silk concentration, but using high molecular weight silks, scaffolds that held their shape were formed using silk concentrations as low as 0.5% wt/v. Silk lamellae thickness decreased with decreasing silk concentration, but high molecular weight silk formed intact lamellae at 0.5% wt/v. The lamellae formed by low molecular weight silks collapsed at these low concentrations, likely due to lack of sufficient molecular entanglement.[24,25] Mechanical properties of lyophilized silk sponges were predominantly a function of silk concentration, but the effect of concentration was greater at low molecular weight compared to that at high molecular weight.

Silk molecular weight distribution was a function of silk fiber degumming time and regenerated silk solutions displayed polydisperse size distribution. Separating silk populations into more distinct molecular weight cutoffs and correlating their size and rheological properties with the final biomaterial characteristics in future studies will provide further insight into the mechanisms that underpin silk assembly and biomaterial formation. However, as a practical consideration, degumming time is a useful parameter to control molecular weight distribution and biomaterial properties. Silk sponges generated in this study had Young's moduli ranging from 37 ± 7.5 kPa to 321.33 ± 49.38 kPa and ultimate tensile strength ranging from 8.7 to 102.7 kPa. The mechanical properties of lyophilized silk sponges were primarily driven by the silk concentration. These stiffness properties are suitable for engineering equivalents of many soft tissues, Stiffness values of soft tissue vary greatly between tissue types, disease state and testing modality, but most mammalian soft tissues have elastic moduli between 0.1 and 100 kPa, values significantly lower than 2D tissue culture plastic and glass substrates that are typically sued to study these tissues in vitro.[26] Although a direct comparison to aqueous salt leached silk scaffolds is difficult because of differences in testing procedures, the lyophilized silk sponges exhibited softer

DOI: 10.1021/ab500149p
ACS Biomater. Sci. Eng. 2015, 1, 260−270

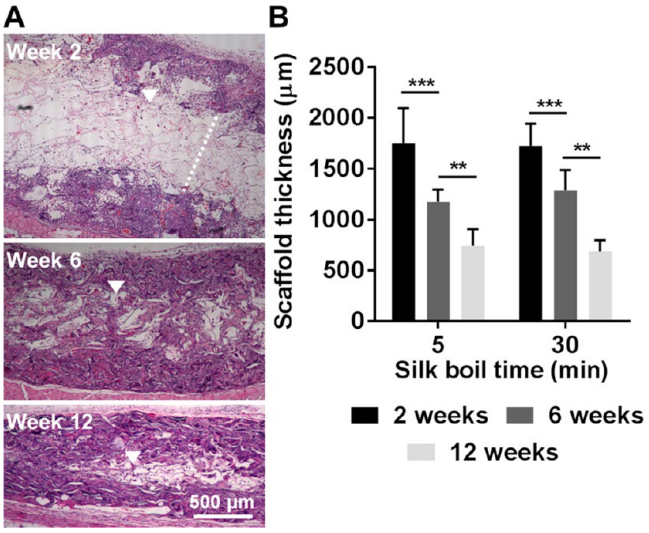

Figure 9. In vivo implantation of lyophilized silk sponges. Lyophilized silk sponges cast from 5 to 60 min degummed silk at 2% wt/v and stabilized by autoclaving were implanted subcutaneously in mice and analyzed histologically at weeks 2, 6, and 12 postimplantation. (A) Representative H&E stained images of scaffolds cast from 5 min degummed silk. Arrows are pointing to intact scaffold regions (i.e., nondegraded), and the dashed line in the first images is showing representative scaffold thickness that was measured in B. (B) Scaffold thickness over time quantified from histology images. Three measurements were made from each end and middle of the section for each sample. Data are expressed as mean ± SD, $n = 5$, ** $p < 0.01$, *** $p < 0.001$.

mechanical properties, as salt leached scaffolds displayed the lowest compressive modulus of 70 kPa at 4% wt/v.[23]

Molecular weight also played a role in determining the mechanical properties of lyophilized silk sponges, with a significant decrease in scaffold stiffness and strength observed with decreased molecular weight. Therefore, although concentration appears to be the main determinant of the mechanical properties of silk scaffolds, tuning the molecular weight adds another dimension to fine-tune the mechanical properties of silk sponges while maintaining scaffold integrity and ease of handling. For example, we showed that silk sponges cast from high molecular weight silk at low concentration (5 min, 0.5% wt/v) and low molecular weight silk at high concentration (60 min, 2% wt/v) have a similar Young's moduli, but high molecular weight scaffolds displayed significantly higher strength and strain at break. Mo and colleagues (2009) have demonstrated that the concentration of reconstituted silk proteins is the governing rheological factor and that silk molecules >50 kDa contribute most to rheological properties of silk solutions degummed for 45 min.[27] In light of this, it would be illuminating to study the rheological features of silk solutions degummed for shorter periods of time and determine if the critical concentration at which silk adopts intramolecular bonding correlates with degumming time and silk molecular weight.

Silk degradation was a function of molecular weight and concentration when silk was stabilized by water annealing (low beta-sheet content). However, at high beta-sheet content, silk degradation rate was lower and other processing parameters (molecular weight, concentration) did not play a significant role. Beta-sheet content is thus the main determinant of silk degradation in vitro, consistent with previous observations in silk films.[15]

hMSCs adhered to and proliferated on all lyophilized silk sponges and scaffold properties did not play a significant role in cell proliferation. Differences in cell morphology were observed at different silk concentrations, with larger, more spread cells observed on high concentration scaffolds. This is consistent with numerous reports of large, spread morphology with distinct actin filaments observed on stiffer substrates.[28−30]

Lyophilize silk sponges implanted in vivo supported cell infiltration from the scaffold periphery. Scaffolds degraded over time, but no obvious differences in the rate of degradation were observed in low-molecular-weight constructs compared to high-molecular-weight constructs. This is consistent with in vitro data, where molecular weight only played a role in scaffold degradation at low beta-sheet content.

5. CONCLUSIONS

A versatile, highly tunable biomaterial platform for soft tissue engineering and regeneration based on lyophilized silk sponges is presented. Compared to salt leached silk scaffolds, this technique provides parameter space with more options for fine-tuning the material properties of silk scaffolds and in particular allows the generation of stable, porous, and soft silk biomaterials for soft tissue engineering and regeneration. Although silk processing parameters showed a high degree of codependence, general trends show that (1) scaffold integrity and handling were improved by increasing the molecular weight of silk, (2) mechanical properties were a function of silk concentration, and (3) scaffold degradation was driven by beta-sheet content.

■ ASSOCIATED CONTENT

Supporting Information

The following file is available free of charge on the ACS Publications website at DOI: 10.1021/ab500149p.

Demonstration of pore interconnectivity via dye movement (PDF)

■ AUTHOR INFORMATION

Corresponding Author

*E-mail: j.rnjak-kovacina@unsw.edu.au.

Notes

The authors declare no competing financial interest.

■ ACKNOWLEDGMENTS

We thank the NIH (NIH P41 EB002520; EY020856), the National Science Foundation Graduate Research Fellowship Program (NSF DGE 0806676), and the Air Force Office of Scientific Research for support. We thank Rachel Stern for her contribution to sponge integrity and degradation studies. As Rachel has completed her studies at Tufts University, we were unable to find her contact details to seek permission to include her as a coauthor on the manuscript. We thank Dr. Chiara E. Ghezzi for her assistance in analyzing the mechanical properties of silk scaffolds.

■ REFERENCES

(1) Lutolf, M. P.; Hubbell, J. A. Synthetic biomaterials as instructive extracellular microenvironments for morphogenesis in tissue engineering. *Nat. Biotechnol.* **2005**, *23*, 47−55.

DOI: 10.1021/ab500149p
ACS Biomater. Sci. Eng. 2015, 1, 260−270

(2) Yuksel, E.; Choo, J.; Wettergreen, M.; Liebschner, M. Challenges in Soft Tissue Engineering. *Semin. Plast. Surg.* **2005**, *19*, 261−270.
(3) Williams, D. *Essential Biomaterials Science*; Cambridge University Press: Cambridge, U.K., 2014.
(4) Engler, A. J.; Sen, S.; Sweeney, H. L.; Discher, D. E. Matrix elasticity directs stem cell lineage specification. *Cell* **2006**, *126*, 677−89.
(5) Orr, A. W.; Helmke, B. P.; Blackman, B. R.; Schwartz, M. A. Mechanisms of mechanotransduction. *Dev. Cell* **2006**, *10*, 11−20.
(6) Omenetto, F. G.; Kaplan, D. L. New Opportunities for an Ancient Material. *Science* **2010**, *329*, 528−531.
(7) Pritchard, E. M.; Kaplan, D. L. Silk fibroin biomaterials for controlled release drug delivery. *Expert Opin. Drug Delivery* **2011**, *8*, 797−811.
(8) Rockwood, D. N.; Preda, R. C.; Yucel, T.; Wang, X. Q.; Lovett, M. L.; Kaplan, D. L. Materials fabrication from Bombyx mori silk fibroin. *Nat. Protoc* **2011**, *6*, 1612−1631.
(9) Nazarov, R.; Jin, H. J.; Kaplan, D. L. Porous 3D scaffolds from regenerated silk fibroin. *Biomacromolecules* **2004**, *5*, 718−726.
(10) Correia, C.; Bhumiratana, S.; Yan, L. P.; Oliveira, A. L.; Gimble, J. M.; Rockwood, D.; Kaplan, D. L.; Sousa, R. A.; Reis, R. L.; Vunjak-Novakovic, G. Development of silk-based scaffolds for tissue engineering of bone from human adipose-derived stem cells. *Acta Biomater.* **2012**, *8*, 2483−2492.
(11) Hofmann, S.; Hilbe, M.; Fajardo, R. J.; Hagenmuller, H.; Nuss, K.; Arras, M.; Muller, R.; von Rechenberg, B.; Kaplan, D. L.; Merkle, H. P.; Meinel, L. Remodeling of tissue-engineered bone structures in vivo. *Eur. J. Pharm. Biopharm* **2013**, *85*, 119−129.
(12) Kim, H. J.; Kim, U. J.; Kim, H. S.; Li, C. M.; Wada, M.; Leisk, G. G.; Kaplan, D. L. Bone tissue engineering with premineralized silk scaffolds. *Bone* **2008**, *42*, 1226−1234.
(13) Mandal, B. B.; Grinberg, A.; Gil, E. S.; Panilaitis, B.; Kaplan, D. L. High-strength silk protein scaffolds for bone repair. *P Natl. Acad. Sci. U.S.A.* **2012**, *109*, 7699−7704.
(14) Wray, L. S.; Rnjak-Kovacina, J.; Mandal, B. B.; Schmidt, D. F.; Gil, E. S.; Kaplan, D. L. A silk-based scaffold platform with tunable architecture for engineering critically-sized tissue constructs. *Biomaterials* **2012**, *33*, 9214−9224.
(15) Hu, X.; Shmelev, K.; Sun, L.; Gil, E. S.; Park, S. H.; Cebe, P.; Kaplan, D. L. Regulation of Silk Material Structure by Temperature-Controlled Water Vapor Annealing. *Biomacromolecules* **2011**, *12*, 1686−1696.
(16) Wray, L. S.; Hu, X.; Gallego, J.; Georgakoudi, I.; Omenetto, F. G.; Schmidt, D.; Kaplan, D. L. Effect of processing on silk-based biomaterials: Reproducibility and biocompatibility. *J. Biomed. Mater. Res. B* **2011**, *99B*, 89−101.
(17) Hu, X.; Kaplan, D.; Cebe, P. Determining beta-sheet crystallinity in fibrous proteins by thermal analysis and infrared spectroscopy. *Macromolecules* **2006**, *39*, 6161−6170.
(18) Huang, W. W.; Krishnaji, S.; Hu, X.; Kaplan, D.; Cebe, P. Heat Capacity of Spider Silk-Like Block Copolymers. *Macromolecules* **2011**, *44*, 5299−5309.
(19) Altman, G. H.; Horan, R. L.; I, M.; Farhadi, J.; Stark, P. R. H.; V, V.; Richmond, J. C.; Vunjak-Novakovic, G.; Kaplan, D. L. Cell differentiation by mechanical stress. *Faseb J.* **2001**, *15*, 270−272.
(20) Brown, J.; Lu, C. L.; Coburn, J.; Kaplan, D. L. Impact of silk biomaterial structure on proteolysis. *Acta Biomater.* **2015**, *11*, 212−221 DOI: 10.1016/j.actbio.2014.09.013.
(21) Gil, E. S.; Park, S. H.; Hu, X.; Cebe, P.; Kaplan, D. L. Impact of sterilization on the enzymatic degradation and mechanical properties of silk biomaterials. *Macromol. Biosci.* **2014**, *14*, 257−69.
(22) Perrone, G. S.; Leisk, G. G.; Lo, T. J.; Moreau, J. E.; Haas, D. S.; Papenburg, B. J.; Golden, E. B.; Partlow, B. P.; Fox, S. E.; Ibrahim, A. M. S.; Lin, S. J.; Kaplan, D. L., The use of silk-based devices for fracture fixation. *Nat. Commun.* **2014**, *5*.10.1038/ncomms4385
(23) Kim, U. J.; Park, J.; Kim, H. J.; Wada, M.; Kaplan, D. L. Three-dimensional aqueous-derived biomaterial scaffolds from silk fibroin. *Biomaterials* **2005**, *26*, 2775−2785.
(24) Inoue, S. I.; Magoshi, J.; Tanaka, T.; Magoshi, Y.; Becker, M. Atomic force microscopy: Bombyx mori silk fibroin molecules and their higher order structure. *J. Polym. Sci. Polym. Phys.* **2000**, *38*, 1436−1439.
(25) Sasithorn, N.; Martinova, L. Fabrication of Silk Nanofibres with Needle and Roller Electrospinning Methods. *J. Nanomater.* **2014**, No. 947315.
(26) Levental, I.; Georges, P. C.; Janmey, P. A. Soft biological materials and their impact on cell function. *Soft Matter* **2007**, *3*, 299−306.
(27) Mo, C. L.; Holland, C.; Porter, D.; Shao, Z. Z.; Vollrath, F. Concentration State Dependence of the Rheological and Structural Properties of Reconstituted Silk. *Biomacromolecules* **2009**, *10*, 2724−2728.
(28) Discher, D. E.; Janmey, P.; Wang, Y. L. Tissue cells feel and respond to the stiffness of their substrate. *Science* **2005**, *310*, 1139−1143.
(29) Wells, R. G. The role of matrix stiffness in regulating cell behavior. *Hepatology* **2008**, *47*, 1394−1400.
(30) Yeung, T.; Georges, P. C.; Flanagan, L. A.; Marg, B.; Ortiz, M.; Funaki, M.; Zahir, N.; Ming, W. Y.; Weaver, V.; Janmey, P. A. Effects of substrate stiffness on cell morphology, cytoskeletal structure, and adhesion. *Cell Motil. Cytoskel.* **2005**, *60*, 24−34.

DOI: 10.1021/ab500149p
ACS Biomater. Sci. Eng. 2015, 1, 260−270